IEEE Access
Multidisciplinary | Rapid Review | Open Access Journal

Date of publication xxxx 00, 0000, date of current version xxxx 00, 0000.

Digital Object Identifier 10.1109/ACCESS.2017.Doi Number

Kalman filter application to GBSAR interferometry for slope monitoring

Alessandra Beni[1], Lapo Miccinesi[1], and Massimiliano Pieraccini[1]

[1]Department of Information Engineering (DINFO), University of Florence, Via Santa Marta 3, 50139 Firenze, Italy

Corresponding author: Alessandra Beni (e-mail: alessandra.beni@unifi.it).

ABSTRACT The use of Kalman filtering techniques for landslide monitoring has proved effective as a tool for estimating and predicting land displacements. Ground-Based Synthetic Aperture Radars (GBSAR) are popular remote sensing instruments able to provide displacement maps of the investigated area, with submillimeter precision. These instruments outperform other sensors in several respects, such as all-weather and all-day monitoring. However, in some cases, for instance in vegetated scenarios, the displacement is affected by a significant uncertainty due to the decorrelation of the radar signal. In such a case, to retrieve any reliable information, noise must be filtered out using appropriate methods. Given the success of kinematic modeling of landslide movements through Kalman filtering, this technique seems to be the optimal candidate for processing the displacement measured by interferometric GBSAR data. This paper investigates this idea, by applying Kalman Filter to GBSAR measurements acquired in two different campaigns: a landslide monitoring in north Spain, and a sliding glacier monitoring in the Alpes, Italy. A proper initialization of the algorithm parameters is fundamental for a correct application of the Kalman filter. In this work, we present a strategy that exploits information from coherent pixels for tuning the filtering parameters and optimizing the filter performance on areas with low coherence.

INDEX TERMS Ground-Based Synthetic Aperture Radar, Interferometry, Landslide Monitoring, Kalman Filter

I. INTRODUCTION

Slope landslide monitoring is a research field of paramount importance for hazard assessment, risk mitigation, and the prevention of natural disasters. Numerous sensors and techniques have been developed for this purpose in recent decades [1]. Field observations of changing topology features, along with in situ ground-based observations, and remote sensing techniques are the three main category of monitoring methods [2].

Among the latter, Ground-Based Synthetic Aperture Radars (GBSAR) achieved success as remote sensing tools for environmental monitoring. GBSAR sensors allow to scan the desired scenario and detect possible displacements of targets in the radar line of sight [3], [4]. The use of interferometric techniques permits to measure targets displacement with an accuracy of a fraction of the signal wavelength. The achievable high resolution coupled with the return time of few minutes, make them optimal candidates for real time monitoring, which is of great importance on active landslides. These sensors are now widely used for environmental monitoring, especially in areas not directly accessible with other instruments [5], [6].

The quality of the interferometric radar data strongly depends on the characteristics of the investigated scenario. For instance, vegetated areas are typically characterized by low coherence [7], [8], i.e., the signal is subject to decorrelation effects, which results in noisier interferometric data. In these cases, standard data interpolation or filtering techniques could lead to an underestimation of the actual result, thus, to a misinterpretation of the data. Therefore, it is of paramount importance to find a way to correctly weight the obtained measurements. To this end, the authors of this article identified the Kalman Filter as a tool to perform dynamic filtering that adequately weights the information coming from consecutive acquisitions. having a method that adequately filters the measured displacements of low coherence pixels would be a valuable resource, as it would improve the deformation detection capability of GBSAR sensors.

The Kalman Filter (KF) [9] is a powerful technique that enables to estimate and predict unknown variables starting

from noisy measurements of a given quantity. It is currently used in several fields, and in a wide range of applications [10], [11], such as orbit calculation, target tracking and navigation. In landslide monitoring the application of KF techniques has recently gained attention, as it proved to be effective in estimating and forecasting ground displacements [12]–[14]. This technique has been applied to displacement measurements acquired with different sensors, and successfully managed to filter out noise and properly predict ground displacement.

Since the last century, KF has been used for Synthetic Aperture Radar (SAR) applications, for addressing the phase unwrapping problem. For instance, authors of [15] proposed the use of KF as a tool to simultaneously unwrap and filter the interferometric phase of the two dimensional SAR image. This approach was based on data fusion of interferometric phase and phase slope information, extracted from the power spectral density of the interferogram. However, this approach did not provide satisfying results in areas of low coherence [16] where, in order to obtain reliable results, an a priori information is needed. This field of application proved successful and efforts are currently been made to optimize this technique, for instance by using an Unscented KF [17], [18].

The KF has been used also for other SAR purposes; for instance authors of [19] proposed a Kalman-filter-based approach to determine 3-D surface deformations by using multisensory, multitrack, and multitemporal SAR interferograms.

Recently, KF was used also in the processing of GBSAR interferometric data [20], [21]. Specifically, in [21] the KF is used to implement a near real-time interferometric analysis with low computational effort. Furthermore, authors of [20] used the KF technique to filter out noise from the timeseries of cumulative displacements obtained with interferometric analysis.

In this paper, we further analyze the application of Kalman filtering techniques to the processing of GBSAR interferometric data. Our intent is to optimize KF to treat noisy, low coherence, pixels in the radar image, which would be discarded for interferometric analysis, so as to retrieve reliable information from them.

One of the main challenges in the application of the KF algorithm, is the parameter initialization. To deal with this task, in this work we propose a procedure based on the so-called Permanent Scatterers [22]. The algorithm parameters are first optimized for these pixels, and then used to treat noisier ones, with appropriate modifications based on the pixel signal noise. This way, it is possible to filter the displacement measured on low coherence pixels in the radar image, and extract information from them.

Compared to the study illustrated in [20], we apply Kalman algorithms to GBSAR measurements acquired in different scenarios, thus, characterized by a great variety of backscattered signals. The case studies reported in this paper are those of a sliding Glacier in the Alpes, Monte Rosa, Italy, and a slow active landslide near Formigal, Spain. These two case studies provide useful insights into the application of Kalman filter on interferometric GBSAR data.

The paper is organized as follows: section II reviews the basic concepts of GBSAR interferometry, while in section III the mathematical formulation of the Kalman filter is presented. Finally, in section IV, the experimental results are presented and discussed.

II. GBSAR INTERFEROMETRY

Interferometry techniques allow to determine the displacement of a target between two radar acquisitions. The displacement is obtained by manipulating the phase of the complex valued GBSAR images. The phase φ of a complex valued image I, relative to a pixel, is the sum of three terms

$$\varphi = \varphi_{dist} + \varphi_{atm} + \varphi_{noise}\,, \tag{1}$$

where φ_{dist} is a phase contribution which depends on the relative distance between radar and the imaged target, φ_{atm} is the phase contribution due to the atmospheric conditions, and φ_{noise} is the noise term. By subtracting the phases of images acquired at different times, we get

$$\Delta\varphi = \Delta\varphi_{dist} + \Delta\varphi_{atm} + \Delta\varphi_{noise}\,. \tag{2}$$

After estimation and removal of the atmospheric contribution, the phase difference is directly related to the target displacement in the radar line of sight, through the equation

$$\Delta d = \frac{\lambda}{4\pi}(\Delta\varphi_{dist} + \Delta\varphi_{noise}), \tag{3}$$

where λ is the wavelength associated to the central frequency of the radar signal. Whether the noise term is present or not determine the possibility of correctly measuring the displacement of a target. In fact, interferometric analysis is usually performed on pixels characterized by high signal quality, for which the noise phase term φ_{noise} in (1) can be considered negligible. For these pixels, by cumulating the displacements retrieved using consecutive GBSAR acquisitions, it is possible to obtain the target movement over time. However, if the noise term greatly affects the interferometric phase, it is difficult to retrieve the correct displacement information. The presence of noise can be due for instance because of residuals of the atmospheric phase screen correction or to non-compensated phase wrapping. The latter effect is common in vegetated scenarios, where decorrelation can cause a loss of phase information, which makes measurement data difficult to interpret.

In order to single out high quality pixels in a GBSAR image, the amplitude dispersion index parameter (D_A) is often used [22], [23]. It can be defined for each pixel of a GBSAR image as

$$D_A = \frac{\sigma_A}{\mu_A}, \tag{4}$$

where σ_A and μ_A are respectively the standard deviation and mean value of the pixel signal amplitude time series. It quantifies the pixel signal quality and is used in radar interferometry to preliminary select candidate areas to carry out the analysis. Indeed, this parameter is related to the corresponding coherence value [24], but is easier to calculate.

The D_A provides us also with an estimation of the displacement measurement error. Indeed, for pixels with sufficiently high signal to noise ratio, the interferometric phase standard deviation can be approximated to the corresponding D_A value [22], [25],

$$\sigma_\varphi \propto D_A. \tag{5}$$

Since σ_φ can be regarded as an estimate of the interferometric phase error, by combining (3) and (5), one can conclude that also the displacement error scales according to the corresponding D_A. This expression has been taken into account for initializing the measurement error parameter of the KF.

III. KALMAN FILTER

In this section the mathematical formulation of the KF algorithm, relative to our case studies, is reviewed.

The FK algorithm allows to estimate/predict an unknown variable $\boldsymbol{x}_k$, possibly multidimensional, at the discrete time k, from a collection $\{z_k\}$ of noisy measurements of a certain quantity. Specifically, the KF consists of two iterative steps: the prediction process and the estimation process.

A. THE PREDICTION PROCESS

The variable $\boldsymbol{x}_k$ to be estimated is called the state variable. In the first phase, the state variable prediction $\tilde{\boldsymbol{x}}_k$, at time k, is determined using the estimate obtained at the previous time step, $\boldsymbol{x}_{k-1}$. To compute this process, a priori information on the evolution of the state variable is required. This information is encapsulated in the state transition equation, which describes the state variable evolution,

$$\boldsymbol{x}_k = f(\boldsymbol{x}_{k-1}) + \boldsymbol{w}_k. \tag{6}$$

Here, f is a linear function that recursively relates the state variable $\boldsymbol{x}_k$ to the state variable at time $k-1$, $\boldsymbol{x}_{k-1}$; $\boldsymbol{w}_k$ is a vector of zero-mean gaussian errors. The variable $\boldsymbol{w}_k$ is called the model error.

In our case the measurements $\{z_k\}$ are the cumulative displacements of a selected target in the scene, obtained using interferometric techniques. The multidimensional variable to be estimated is composed by the position and velocity components of the displacement in the radar line of sight, relative to the selected pixel, at time k. That is, $\boldsymbol{x}_k = (p_k, v_k)^T$.

The linear function f represents the kinematic model describing the target movement. In the case studies analyzed in this paper, we are interested in the ground displacement due to the sliding of a glacier or a landslide.

In both cases, the ground motion results from the sum of gravitational and frictional forces acting on the selected target of the slope/glacier. Furthermore, in interferometric analysis a single pixel is monitored during a certain period. Therefore, the retrieved displacement is relative to a point of the scenario with fixed coordinates. The point is characterized by a constant inclination. Thus, in most cases, the dynamics will evolve towards a stationary situation, where the ground is subject to constant motion. In this case, the function f can be written in matrix form as,

$$A = \begin{pmatrix} 1 & \Delta t \\ 0 & 1 \end{pmatrix}, \tag{7}$$

where Δt is the value of the time interval between successive acquisitions.

From a practical viewpoint, the prediction process of the KF algorithm consists of two steps; the computation of the state variable prediction $\tilde{\boldsymbol{x}}_k$, and the computation of the covariance state variable prediction $\tilde{P}_k$. The state variable prediction for the k-th time step, is given by the transition equation

$$\tilde{\boldsymbol{x}}_k = A\boldsymbol{x}_{k-1}, \tag{8}$$

with matrix A defined in (7), and $\mathbf{x}_{k-1}$ the final estimate from the previous iterative step. The prediction of the state variable covariance matrix is given by

$$\tilde{P}_k = AP_{k-1}A^T + Q, \tag{9}$$

where the matrix Q is the covariance of the model error $\boldsymbol{w}_k$. If a white noise acceleration model is assumed [14], [25], [26], the Q matrix is equal to

$$Q = \sigma_w^2 \begin{pmatrix} \Delta t^4/4 & \Delta t^3/2 \\ \Delta t^3/2 & \Delta t \end{pmatrix}, \tag{10}$$

Where Δt is the time interval between consecutive acquisitions, and σ_w^2 is the covariance of the white noise acceleration process. One of the main challenges to properly apply KF, is the choice of σ_w^2.

B. THE ESTIMATION PROCESS

In the estimation process the measurement z_k is used to correct the prediction $\tilde{\boldsymbol{x}}_k$, and to obtain the final estimate $\boldsymbol{x}_k$. In fact, each element z_k of the measurement collection, is related to the variable $\boldsymbol{x}_k$, through the so-called measurement equation

$$z_k = h(\boldsymbol{x}_k) + e_k, \tag{11}$$

where e_k is a zero-mean gaussian error, called the measurement error, whose variance is $R = \sigma_e^2$.

The estimation process involves three steps: the computation of the so-called Kalman gain K_k, the correction of the prediction estimate $\tilde{\boldsymbol{x}}_k$ to get the final estimate $\boldsymbol{x}_k$, and the correction of the covariance prediction. The Kalman Gain is given by the following expression

$$K_k = \tilde{P}_k H^T \left(H\tilde{P}_k H^T + R\right)^{-1}. \tag{12}$$

Here, H is the state-to-measurement vector, which in our case is equal to

$$H = (1 \quad 0), \tag{13}$$

R is the covariance of the measurement error e_k, and $\tilde{P}_k$ is the prediction of the state variable covariance matrix, calculated in (9).

The correction of the predicted value $\tilde{\boldsymbol{x}}_k$ is realized by properly weighting the deviation of the measurement z_k from the predicted value, with the Kalman gain. Specifically, the final estimate of the state variable is given by

$$\boldsymbol{x}_k = \tilde{\boldsymbol{x}}_k + K_k(z_k - H\tilde{\boldsymbol{x}}_k). \tag{14}$$

Finally, the correction of the covariance prediction is calculated with the following expression

$$P_k = \tilde{P}_k - K_k H \tilde{P}_k. \tag{15}$$

C. PARAMETERS INITIALIZATION

The performance of the KF mainly depends on the choice of the state transition kinematic model (the matrix A), and on the model and measurement error covariance Q and R, whose values must be initialized *a priori*. Therefore, once the kinematic model is selected, the performance of the algorithm strongly depends on the choices made for the error covariances Q and R. Changing one of this two quantities, dramatically modifies the filter result. Specifically, once the value of R is fixed, increasing Q means that the kinematic model is more influenced by the error. Thus, in calculating the final estimate, the filter gives more relevance to the measurement outcomes. On the other hand, by decreasing Q values, the filter relies more on the dynamic model entering the state transition equation. As a result, the measurement outcomes have less weight in the final estimate. The initialization of the error covariance parameters determines the success or failure of the filtering procedure. Unfortunately, there is not a universal standard for initializing Q and R values, but they must be tuned case by case, depending on the signal and scenario characteristics. Care must be taken in this choice, since in some cases, place too little or too much weight to the experimental measurements, can lead to a loss of information.

In fact, like many other filtering algorithms, KF can lead to excessive filtering of the variable of interest. To solve this issue, the first setting of the parameters must be performed by an operator who, on the basis of a priori knowledge of the physical scenario under investigation, can determine whether the result is reliable or not.

To address the challenging choice of model and error covariances and avoid over-filtering, in this work the KF is first applied to a coherent group of pixels for optimizing the filtering parameters. Indeed, these high quality pixels can be considered as benchmarks, for which the corresponding measured displacement is reliable. When KF is applied to coherent pixels, we keep fixed the R value, determined by the sensor uncertainty, and optimize the Q parameter according to the scenario characteristics. For GBSAR sensors the theoretical measurement uncertainty on high quality pixels, in an optimal scenario, is of the order of 0.1 mm [27]. However, especially in natural scenarios, many factors introduce additional sources of uncertainty. For instance, natural environments are in general characterized by a lower reflectivity. Moreover, the large distance of targets from the sensor, leads to a decrease in the intensity of the backscattered signal, hence, to a decrease of the signal to noise ratio. For these reasons, we estimated the measurement uncertainty directly from the scenario under investigation, as the average of the standard deviation of the displacement of coherent pixels of the scenario. Doing so, we obtained a measurement uncertainty of the order of 1 mm. Nevertheless, we experienced no substantial deviation by tuning the measurement uncertainty σ_e from 0.1 mm to 1 mm, as can be seen in Figure 1. In this figure, we show results of KF filtering of a measured interferometric displacement, with fixed Q, and $\sigma_e = 0.1\,mm$ and $\sigma_e = 1\,mm$. This evidences that the algorithm is robust to a fine tuning of the R parameter within this range.

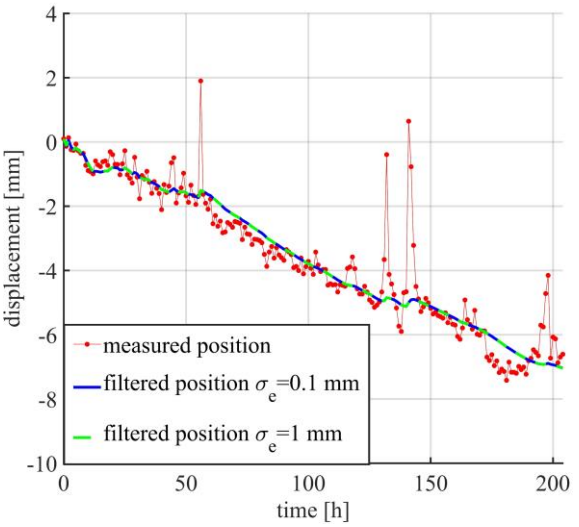

FIGURE 1. Example of filtered displacement trend obtained with different values for the measurement uncertainty. Red dots represent the measurement outcomes from interferometric analysis, dashed blue and green lines the filtered variables obtained with $\sigma_e = 0.1\,mm$ and $\sigma_e = 1\,mm$, respectively.

We then proceed as follows: by keeping fixed the R value, determined by $\sigma_e = 1\,mm$, we are able to properly tune σ_w^2, and hence, Q values, considering high quality pixels. Once determined the proper choice for Q for the investigated scenario, we apply KF to noisier pixels in the image. This time, we keep the Q parameter constant, and tune the measurement error variance R, according to the noise that affects the data, based on (5).

IV. EXPERIMENTAL RESULTS

In order to study the applicability of KF techniques to GBSAR interferometric data, measurements acquired in two different

scenarios have been analyzed. They were obtained in measurement campaigns performed on Monte Rosa, near the village of Macugnaga, Italy, and near Formigal, Spain.

Our purpose is to use the KF to extrapolate displacement information from noisy pixels with low signal quality, by tuning the algorithm parameters based on the information retrieved from high quality neighboring pixels. As already said, to identify high- and low-quality pixels we used the D_A parameter. Pixels whose D_A is less than 0.15 are identified as stable targets, whose signal has a high quality.

A. MACUGNAGA CASE STUDY

The objective of the Macugnaga measurement campaign was to test the ability of a GBSAR system working in C-band, to monitor a sliding glacier. The sensor was able to acquire an image almost each 30 minutes.

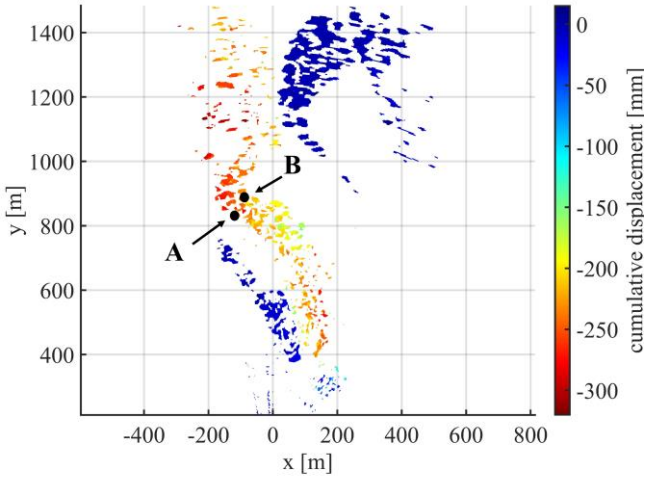

FIGURE 2. Map of cumulative displacements calculated using interferometric techniques, in the Macugnaga campaign. Black dots indicate the targets used for the analysis.

Fig. 2 shows a map of cumulative displacements of the scenario, retrieved from interferometric analysis, performed over a time series lasting about 5 days. Before performing the interferometric analysis, the atmospheric phase component was estimated and compensated by using a linear range model.

Fig. 2 was obtained by applying a threshold on D_A values. Only pixels with $D_A < 0.4$ appear in the image. The part of the glacier which is sliding is clearly visible. In this case the movement is rapid, at a speed of about 2 cm per hour.

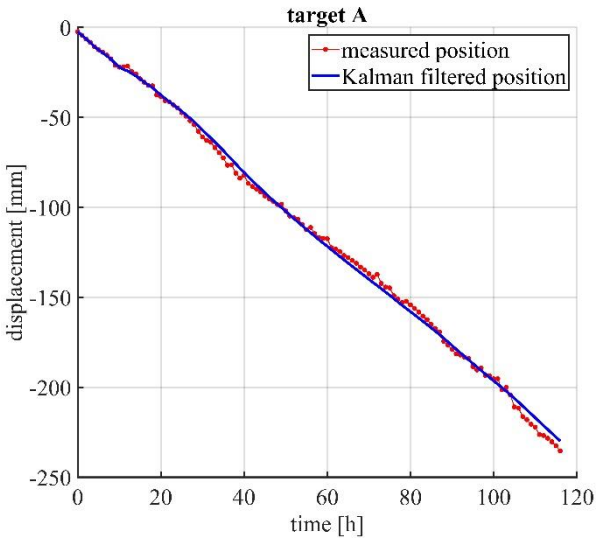

FIGURE 3. Displacement trend over time obtained for target A, of the glacier scenario. Red dots represent the displacement measurement outcomes from interferometric analysis, while the blue line is the result of the Kalman Filter with $\sigma_w = 3.6\ \mathrm{mm/min^2}$.

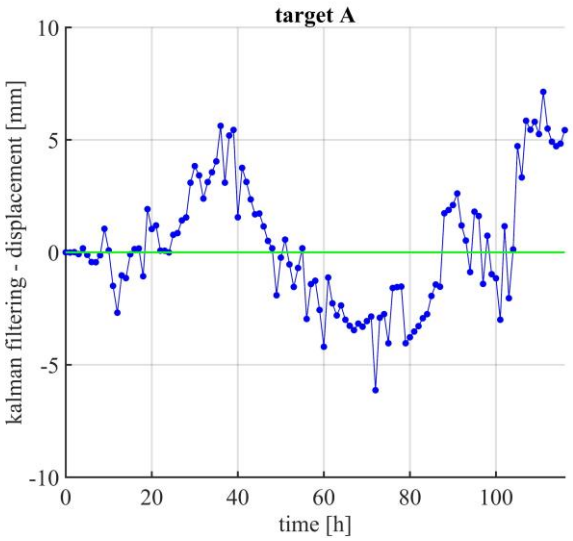

FIGURE 4. Blue dots represent the residual between displacement measured value and the corresponding filtered quantity, obtained for target A and $\sigma_w = 3.6\ \mathrm{mm/min^2}$. The green line highlights the perfect agreement.

In this scenario, we selected pixels with different features. In what follows we show the results obtained for a stable pixel, with $D_A = 0.11$ (target A in Fig. 2), and a pixel with $D_A = 0.35$ (target B in Fig. 1), at about the same range value. We calculated the displacement of the targets over time, using the cumulative interferometric phase according to (3).

Fig. 3 shows the result obtained for target A by applying the KF to the measured displacement over time. The blue line represents the filtered variable, while the red points represent the measured displacement before filtering. In this case, the variable σ_w which defines the Q covariance matrix was set equal to 3.6 $\mathrm{mm/min^2}$. It can be noted that, the blue line representing the filtered displacement over time, partially

deviates from the measured values. This is better evidenced by the results shown in Fig. 4, where the deviation of filtered values from the measured ones is represented. The residual clearly shows systematic behaviour. This suggests that this filter does not adequately reproduce real motion. In this case, the model has been assigned too much weight with respect to the measurements. Therefore, we repeated the filtering procedure by increasing the Q values, in order to give greater relevance to the measurements. The obtained results are shown in Fig. 5 and Fig. 6, for $\sigma_w = 36\ \mathrm{mm/min^2}$. In this case, the measurement trend is better reproduced, despite the noise being filtered, and the residuals appear symmetric, which suggests a more reliable estimation.

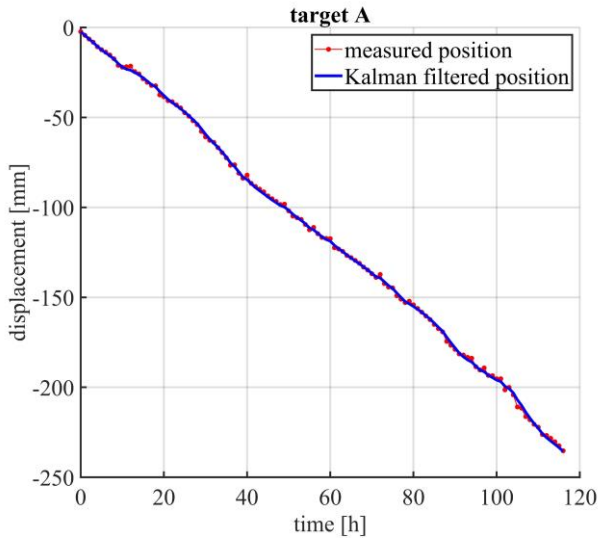

FIGURE 5. **Displacement trend over time obtained for target A, of the glacier scenario. Red dots represent the displacement measurement outcomes from interferometric analysis, while the blue line is the result of the Kalman Filter with $\sigma_w = 36\ \mathrm{mm/min^2}$.**

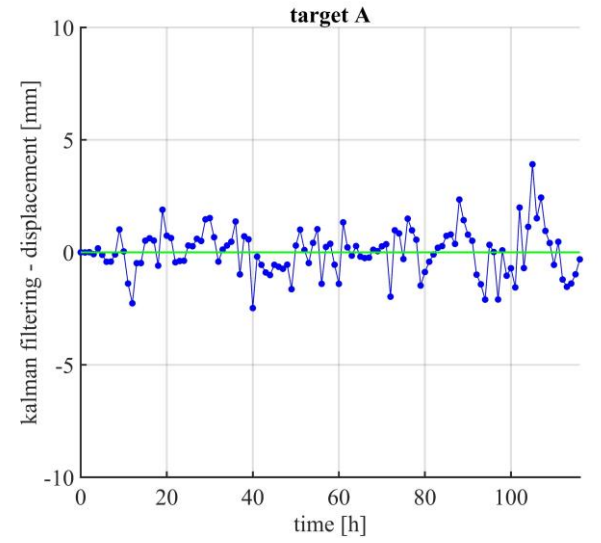

FIGURE 6. **Blue dots represent the residual between displacement measured value and the corresponding filtered quantity, obtained for target A and $\sigma_w = 36\ \mathrm{mm/min^2}$. The green line highlights the perfect agreement.**

Once optimized the KF parameters, for high quality pixels of the scenario, we repeated the processing for low coherence pixels, by scaling the measurement error variance R, based on the corresponding D_A value, according to (5). Fig. 7 shows the results obtained for target B (see Fig. 2). In this case, the measured displacement was noisier, and the filter successfully reduced the noise.

Since this scenario was subject to a rapid movement, the displacement trend was already evident even before the filtering operation. However, the filtered displacement is smoother, as the KF is able to filter out non-physical fluctuations.

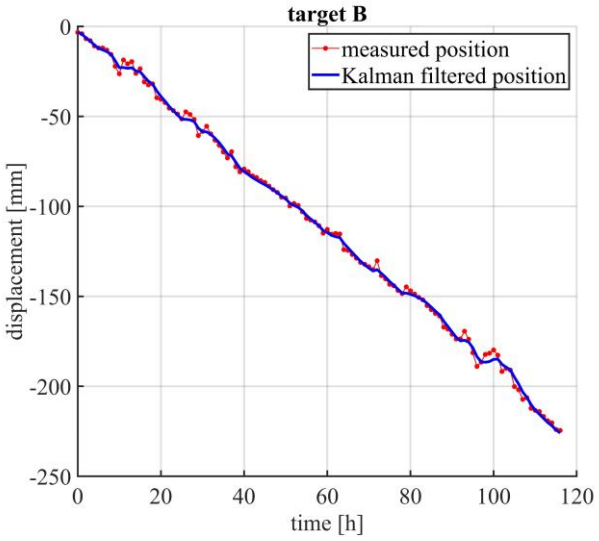

FIGURE 7. **Displacement trend over time obtained for target B, of the glacier scenario. Red dots represent the displacement measurement outcomes from interferometric analysis, while the blue line is the result of the Kalman Filter with $\sigma_w = 36\ \mathrm{mm/min^2}$.**

B. FORMIGAL CASE STUDY

To further test the performance of the proposed method, we analyzed a second series of GBSAR measurements, acquired in Spain, near Formigal, with a C-band system. The system return time was of about one hour. Aim of the experimental campaign was to monitor a slope landslide, just above a road. In this case, the slope was subject to a slow movement, with a velocity of about 1 mm per day. Moreover, the slope was partially covered by grass and low vegetation. These two aspects make this scenario the perfect candidate for our study, as it comprises both high- and low-quality pixels, subject to slow movements, hence, more difficult to measure.

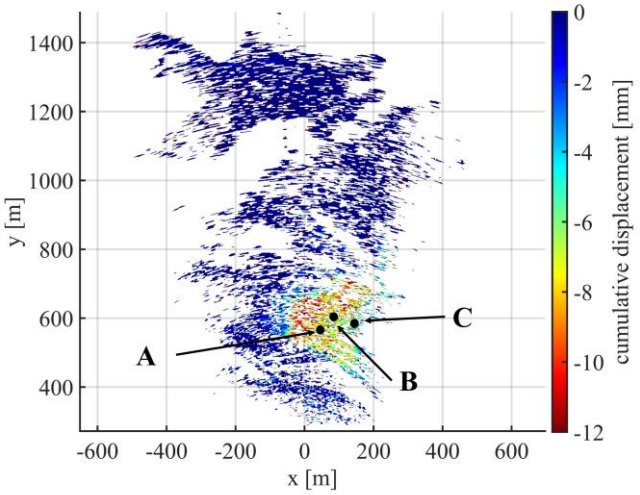

FIGURE 8. **Map of cumulative displacements calculated using interferometric techniques, in the Formigal campaign. Black dots indicate the targets used for the analysis.**

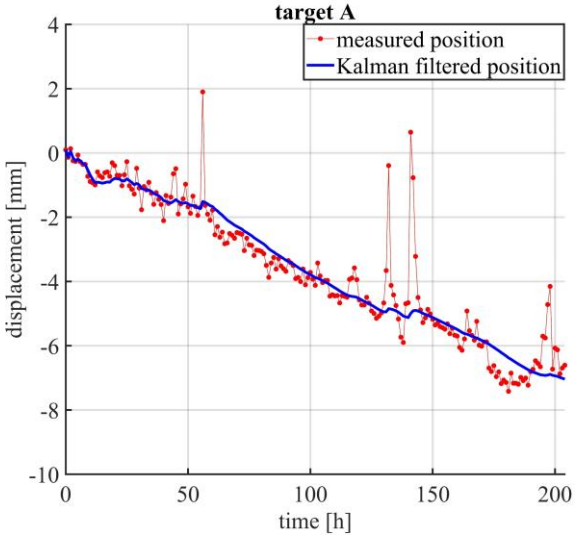

FIGURE 9. **Displacement trend over time obtained for target A, of the slope landslide scenario. Red dots represent the displacement measurement outcomes from interferometric analysis, while the blue line is the result of the Kalman Filter with $\sigma_w = 0.04\ \mathrm{mm/min^2}$.**

Fig. 8 shows the cumulative displacement map, obtained using interferometric techniques, after atmospheric phase compensation, for a time series lasting 8 days. Only pixels with $D_A < 0.4$ are shown in the image.

As done for the Macugnaga case study, KF was applied first to high quality pixels, in order to optimize the algorithm parameters for this scenario. Here, we report the results obtained for target A (see Fig. 8), which has $D_A = 0.15$. Fig. 9 shows the result of the filtering operation once the parameter Q has been optimized for this scenario. In this case, the covariance noise model σ_w has been set equal to 0.04 $\mathrm{mm/min^2}$. Fig. 10 shows the residual between the measured and filtered displacements.

Once optimized the algorithm parameters, the KF was applied to noisier targets, characterized by a higher D_A. As done for the Macugnaga case study analysis, the R parameter was tuned according to the D_A value of the pixels. In Fig. 11 and Fig.12 we show the results obtained for target B ($D_A = 0.39$), and target C ($D_A = 0.33$), respectively. In both cases, it can be seen that the measured displacements (red dots) are much noisier. For these targets, without any filtering operation, it is not easy to identify which is the displacement trend over time. On the other hand, the filtered variables clearly outline a decreasing trend in the target position over time. It is worth noting that target B and C present different displacement velocity. These results suggest that the algorithm can successfully be applied to pixels subject to different deformation rate.

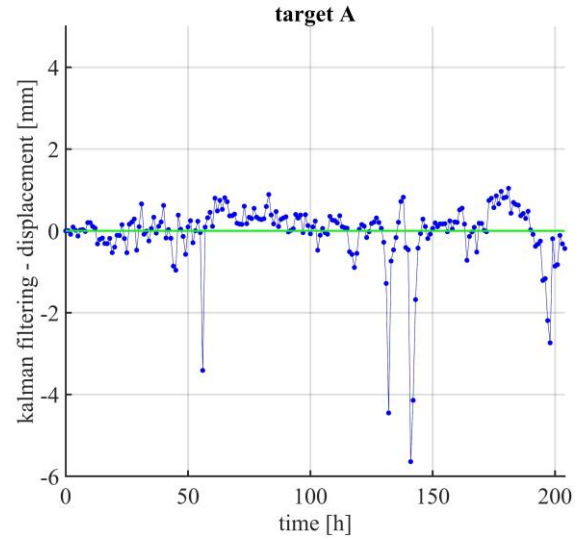

FIGURE 10. **Blue dots represent the residual between displacement measured value and the corresponding filtered quantity, obtained for target A and $\sigma_w = 0.04\ \mathrm{mm/min^2}$. The green line highlights the perfect agreement.**

It must be noticed that for short time intervals (for instance time below 20 hours in Fig. 11), the filtered displacement trend shows a probably non-physical peak. However, for times beyond 20 hours, such peaks are less and less pronounced. This is because the KF algorithm relies on the pixel's displacement history and, in case of noisier measurements, it takes longer to converge. Therefore, in case of low coherence pixels care must be taken when starting to trust the filtering result. For instance, in case of target B (Fig. 11), measurements acquired in the first 20 hours should be discarded for the analysis. However, this is not a problem for modern instrumentations, which have acquisition rates of the

order of minutes. Indeed, modern sensors can acquire enough measurements for the algorithm to gather information about the movement history and, thus, converge within few hours.

These results show that by using the KF it is possible to extract displacement information also from noisy pixels, which would have been discarded for standard interferometric analysis.

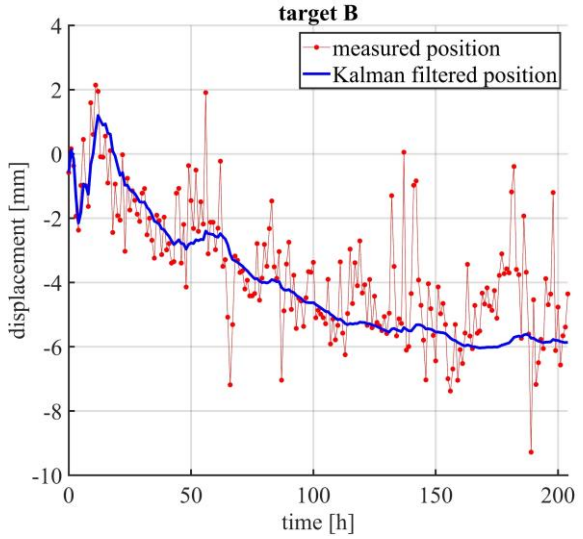

FIGURE 11. Displacement trend over time obtained for target B, of the slope landslide scenario. Red dots represent the displacement measurement outcomes from interferometric analysis, while the blue line is the result of the Kalman Filter with $\sigma_w = 0.04\ \mathrm{mm/min^2}$.

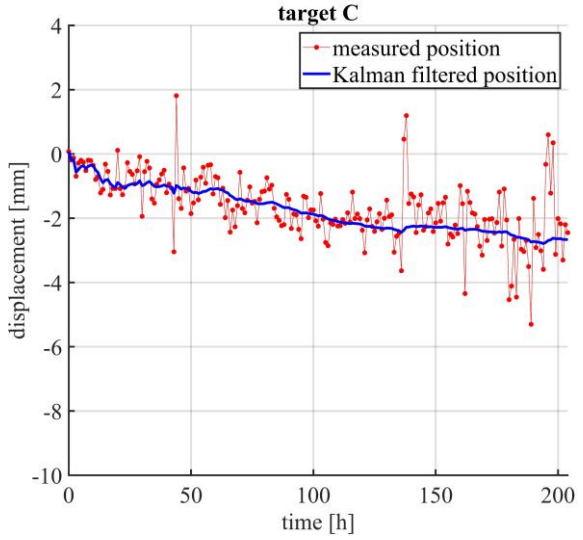

FIGURE 12. Displacement trend over time obtained for target C, of the slope landslide scenario. Red dots represent the displacement measurement outcomes from interferometric analysis, while the blue line is the result of the Kalman Filter with $\sigma_w = 0.04\ \mathrm{mm/min^2}$.

V. CONCLUSIONS

This work explores the possibility of using the Kalman filter as a tool to extract displacement information from low-coherent pixels of a GBSAR image.

The mathematical formulation of the Kalman filter is examined and the application to cumulative interferometric radar data is discussed. Particular attention is paid to the correct way to initialize the algorithm parameters. Specifically, we implement a procedure to optimize KF parameters to treat low coherence areas, based on information from few high-quality pixels.

The method is tested on data resulting from GBSAR measurement campaigns representative of two different scenarios: a sliding fast moving glacier, and a slow-moving slope covered by grass.

The results obtained show that in both situations the KF successfully filters out noise and outlines a clear trend for the targets position over time. The algorithm proved to be robust for the application on noisy targets and targets subject to displacements of different intensity. This method can be used to extract useful information from areas characterized by low coherence, improving the performance of GBSAR measurements in slope monitoring.

REFERENCES

[1] S. Uhlemann *et al.*, 'Assessment of ground-based monitoring techniques applied to landslide investigations', *Geomorphology*, vol. 253, pp. 438–451, Jan. 2016, doi: 10.1016/j.geomorph.2015.10.027.

[2] B.-G. Chae, H.-J. Park, F. Catani, A. Simoni, and M. Berti, 'Landslide prediction, monitoring and early warning: a concise review of state-of-the-art', *Geosci J*, vol. 21, no. 6, pp. 1033–1070, Dec. 2017, doi: 10.1007/s12303-017-0034-4.

[3] Y. Wang *et al.*, 'Ground-Based Differential Interferometry SAR: A Review', *IEEE Geoscience and Remote Sensing Magazine*, vol. 8, no. 1, pp. 43–70, Mar. 2020, doi: 10.1109/MGRS.2019.2963169.

[4] O. Monserrat, M. Crosetto, and G. Luzi, 'A review of ground-based SAR interferometry for deformation measurement', *ISPRS Journal of Photogrammetry and Remote Sensing*, vol. 93, pp. 40–48, Jul. 2014, doi: 10.1016/j.isprsjprs.2014.04.001.

[5] D. Tarchi *et al.*, 'Landslide monitoring by using ground-based SAR interferometry: an example of application to the Tessina landslide in Italy', *Engineering Geology*, vol. 68, no. 1, pp. 15–30, Feb. 2003, doi: 10.1016/S0013-7952(02)00196-5.

[6] L. Noferini *et al.*, 'Using GB-SAR technique to monitor slow moving landslide', *Engineering Geology*, vol. 95, no. 3, pp. 88–98, Dec. 2007, doi: 10.1016/j.enggeo.2007.09.002.

[7] A. Monti-Guarnieri, M. Manzoni, D. Giudici, A. Recchia, and S. Tebaldini, 'Vegetated Target Decorrelation in SAR and Interferometry: Models, Simulation, and Performance Evaluation', *Remote Sensing*, vol. 12, no. 16, Art. no. 16, Jan. 2020, doi: 10.3390/rs12162545.

[8] H. A. Zebker and J. Villasenor, 'Decorrelation in interferometric radar echoes', *IEEE Transactions on Geoscience and Remote Sensing*, vol. 30, no. 5, pp. 950–959, Sep. 1992, doi: 10.1109/36.175330.

[9] R. E. Kalman, 'A New Approach to Linear Filtering and Prediction Problems', *Journal of Basic Engineering*, vol. 82, no. 1, pp. 35–45, Mar. 1960, doi: 10.1115/1.3662552.

[10] F. Auger, M. Hilairet, J. M. Guerrero, E. Monmasson, T. Orlowska-Kowalska, and S. Katsura, 'Industrial Applications of the Kalman Filter: A Review', *IEEE Transactions on Industrial Electronics*, vol. 60, no. 12, pp. 5458–5471, Dec. 2013, doi: 10.1109/TIE.2012.2236994.

[11] Q. Li, R. Li, K. Ji, and W. Dai, 'Kalman Filter and Its Application', in *2015 8th International Conference on Intelligent Networks and Intelligent Systems (ICINIS)*, Nov. 2015, pp. 74–77. doi: 10.1109/ICINIS.2015.35.

[12] F. Lu and H. Zeng, 'Application of Kalman Filter Model in the Landslide Deformation Forecast', *Sci Rep*, vol. 10, no. 1, Art. no. 1, Jan. 2020, doi: 10.1038/s41598-020-57881-3.
[13] N. Zhang, W. Zhang, K. Liao, H. Zhu, Q. Li, and J. Wang, 'Deformation prediction of reservoir landslides based on a Bayesian optimized random forest-combined Kalman filter', *Environ Earth Sci*, vol. 81, no. 7, p. 197, Mar. 2022, doi: 10.1007/s12665-022-10317-9.
[14] S. Gamse, 'Dynamic modelling of displacements on an embankment dam using the Kalman filter', *Journal of Spatial Science*, vol. 63, no. 1, pp. 3–21, Jan. 2018, doi: 10.1080/14498596.2017.1330711.
[15] O. Loffeld and R. Kramer, 'Phase unwrapping for SAR interferometry. A data fusion approach by Kalman filtering', in *IEEE 1999 International Geoscience and Remote Sensing Symposium. IGARSS'99 (Cat. No.99CH36293)*, Jun. 1999, vol. 3, pp. 1715–1717 vol.3. doi: 10.1109/IGARSS.1999.772071.
[16] H. Nies, O. Loffeld, and R. Wang, 'Phase Unwrapping using 2D-Kalman Filter - Potential and Limitations', in *IGARSS 2008 - 2008 IEEE International Geoscience and Remote Sensing Symposium*, Jul. 2008, vol. 4, p. IV-1213-IV–1216. doi: 10.1109/IGARSS.2008.4779947.
[17] Y. Gao, S. Zhang, T. Li, Q. Chen, S. Li, and P. Meng, 'Adaptive Unscented Kalman Filter Phase Unwrapping Method and Its Application on Gaofen-3 Interferometric SAR Data', *Sensors*, vol. 18, no. 6, Art. no. 6, Jun. 2018, doi: 10.3390/s18061793.
[18] X. Xie and Y. Pi, 'Phase noise filtering and phase unwrapping method based on unscented Kalman filter', *Journal of Systems Engineering and Electronics*, vol. 22, no. 3, pp. 365–372, Jun. 2011, doi: 10.3969/j.issn.1004-4132.2011.03.001.
[19] J. Hu, X.-L. Ding, Z.-W. Li, J.-J. Zhu, Q. Sun, and L. Zhang, 'Kalman-Filter-Based Approach for Multisensor, Multitrack, and Multitemporal InSAR', *IEEE Transactions on Geoscience and Remote Sensing*, vol. 51, no. 7, pp. 4226–4239, Jul. 2013, doi: 10.1109/TGRS.2012.2227759.
[20] A. Tan, Z. Tan, W. Tian, M. Yan, and Y. Long, 'Application of Kalman Filter in Deformation Data Processing of Ground-based Differential Interferometric Radar', in *2019 IEEE International Conference on Signal, Information and Data Processing (ICSIDP)*, Dec. 2019, pp. 1–5. doi: 10.1109/ICSIDP47821.2019.9173304.
[21] S. Roedelsperger, M. Becker, C. Gerstenecker, and G. Laeufer, 'Near Real-Time Monitoring of Displacements with the Ground Based SAR IBIS-L', vol. 677, p. 64, Mar. 2010.
[22] A. Ferretti, C. Prati, and F. Rocca, 'Permanent scatterers in SAR interferometry', *IEEE Transactions on Geoscience and Remote Sensing*, vol. 39, no. 1, pp. 8–20, Jan. 2001, doi: 10.1109/36.898661.
[23] M. Crosetto, O. Monserrat, M. Cuevas-González, N. Devanthéry, and B. Crippa, 'Persistent Scatterer Interferometry: A review', *ISPRS Journal of Photogrammetry and Remote Sensing*, vol. 115, pp. 78–89, May 2016, doi: 10.1016/j.isprsjprs.2015.10.011.
[24] A. Beni, L. Miccinesi, A. Michelini, and M. Pieraccini, 'Temporal Coherence Estimators for GBSAR', *Remote Sensing*, vol. 14, no. 13, Art. no. 13, Jan. 2022, doi: 10.3390/rs14133039.
[25] S. Rödelsperger, *Real-time processing of ground based synthetic aperture radar (GB-SAR) measurements*. Darmstadt: Techn. Univ., Geodätisches Inst, 2011.
[26] Y. Bar-Shalom, X. Li, and T. Kirubarajan, 'Estimation with Applications to Tracking and Navigation: Theory, Algorithms and Software', 2001. doi: 10.1002/0471221279.
[27] M. Pieraccini, M. Fratini, F. Parrini, C. Atzeni, and G. Bartoli, 'Interferometric radar vs. accelerometer for dynamic monitoring of large structures: An experimental comparison', *NDT & E International*, vol. 41, no. 4, pp. 258–264, Jun. 2008, doi: 10.1016/j.ndteint.2007.11.002.

ALESSANDRA BENI was born in Florence, Italy, in 1993. She received the B.S. degree in Physics and the M.S. degree in Theoretical Physics from the University of Florence, Florence, Italy, in 2016 and in 2019, respectively.

She is currently attending the second year of the PhD program in Information Engineering of the University of Florence, Florence, Italy. Her research interests include radar interferometry, radar data processing, ground-based radars, ground-based synthetic aperture radars, and ground penetrating radars.

LAPO MICCINESI was born in Florence, Italy, in 1988. He received the B.S. degree in physics and M.S. degree in physics of particles from the University of Florence, Florence, in 2011 and 2016, respectively, and Ph.D. degree in information engineering from the University of Florence, Florence, Italy in 2020.

He is currently with the Department of Information Engineering, University of Florence, as a Post-Degree Grant Recipient. His research interests include ground penetrating radar, radar interferometry, ground-based radar, and ground-based synthetic aperture radar.

MASSIMILIANO PIERACCINI received the M.S. degrees in Physics from the University of Florence, Firenze, Italy, in 1994 and the Ph.D. degree in Non-destructive Testing from University of Florence, Firenze, Italy, in 1998.

From 1997 to 2005, he was a Research Assistant with Department of Electronics and Telecommunications (former Department of Electronic Engineering) at the University of Florence, Firenze, Italy. From 2005 to 2020, he was an Associate Professor, and since 2020 he has been Full Professor with the same Department (now Department of Information Engineering). Currently, he is President of Electronic Engineering School of University of Florence. He is the author of four books, more than 170 articles, and more than 9 patented inventions. His research interests include ground penetrating radar, ground-based synthetic aperture radar, interferometric radar, microwave sensors.